Alexandria Engineering Journal (2022) xxx, xxx–xxx

HOSTED BY

Alexandria University

Alexandria Engineering Journal

www.elsevier.com/locate/aej
www.sciencedirect.com

Damage analysis of a CFRP cross-ply laminate subjected to abrasive water jet cutting

Murat Demiral [a,*], **Fethi Abbassi** [a,*], **Tamer Saracyakupoglu** [b], **Mohamed Habibi** [c]

[a] *College of Engineering and Technology, American University of the Middle East, Kuwait*
[b] *Turkish Aerospace Industries, 06980 Ankara, Turkey*
[c] *Departement of Mechanical Engineering, Université du Québec à Trois-Rivières, Quebec, Canada*

Received 30 October 2021; revised 1 January 2022; accepted 3 January 2022

KEYWORDS

Abrasive water jet cutting;
CFRP laminate;
Delamination;
Matrix cracking;
SPH method

Abstract The abrasive water jet (AWJ) cutting technique is one of the promising techniques used in machining of composite materials due to lack of thermal damage, lower tool wear and higher productivity. In this study, the AWJ cutting of a cross-ply CFRP laminate was investigated experimentally and numerically. The purpose is to understand the underlying physics of the AWJ cutting of a composite plate, which can be later used to control the process as well as optimizing its parameters. In the performed tests of the plate with a stacking sequence of [0°/90°/0°/90°] and having a total thickness value of 0.84 mm, where the pressure of particles and impact angle were varied, different failure characteristics such as fiber pull-out, fiber breakage, fiber debonding, matrix cracking and delamination were noticed. A three-dimensional FE model of the process was developed using ABAQUS finite element software to understand the underlying physics. In the model, the pure water jet particles following the linear Hugoniot form of the Mie-Grüneisen equation of state and highly rigid abrasive particles were modelled using smooth particle hydrodynamics. While the three dimensional Hashin damage model was used to simulate the intra ply damage, cohesive zone elements were used to predict the delamination. The damage characteristics in the composite plate was investigated for different process parameters. When the speed of the AWJ particles increased from 300 m/s to 600 m/s, the amount of delamination decreased from 6.44% to 5.69% at the top interface with no more delamination observed at the middle and bottom interfaces. The delamination performance of 0°/90°/0°/90° orientation was found to be better than those of 0°/90°/90°/0° and 0°/0°/90°/90° orientations. The impact angle of the particles affected the material removal rate in the process significantly. The failure behaviour of the laminate subjected to AWJ and pure water jet cuttings (PWJ) were also compared.

* Corresponding authors.
E-mail addresses: Murat.Demiral@aum.edu.kw (M. Demiral), Fethi.abbassi@aum.edu.kw (F. Abbassi).

Peer review under responsibility of Faculty of Engineering, Alexandria University.

https://doi.org/10.1016/j.aej.2022.01.018

Nomenclature

AWJ	Abrasive water jet	ρ	Mass density(Kg/m^3)
PWJ	Pure water jet	c_0	Speed of sound (m/s)
FEM	Finite element modeling	η	Nominal volumetric compressive strain
CFRP	Carbon-fiber-reinforced polymers	U_s	Shock velocity
FSI	Fluid-structure interaction	U_p	Particle velocity
SEM	Scanning electron microscopy	E_m	Internal energy the internal energy per unit mass
SPH	Smoothed particle hydrodynamics	mt	Matrix tension
CZM	Cohesive zone method	mc	Matrix compression
EOS	Equation of state	ft	Fiber tension
CFD	Computational fluid dynamics	fc	Fiber compression
V	Speed of particles (m/s)	s	Material constant
α	Impact angles of water jet particles (°)	Γ_0	Material constant
p	Pressure stress (Mpa)		

1. Introduction

Composite materials have been increasingly used to manufacture sophisticated products requiring lightweight and higher strength to resist complex loadings in challenging environments [1,2]. Due to their higher prices, their products are restricted to be used mostly in advanced engineering fields such as space, aircraft, boat and automotive. Carbon Fibre Reinforced Polymer (CFRP) composite is well known for being a challenging material to be machined using traditional methods due to their heterogeneous nature where the strong fibers are embedded into a softer matrix [3]. The conventional machining technique does, in fact, have heat effects [4]. The abrasive water jet (AWJ) is one of the promising techniques used for machining various materials including composites using a high-pressure jet of water. In this process, high-velocity water containing abrasive particles is used to cut different materials ranging from ductile to brittle. It is capable of producing sharp corners, processing shapes with small radii, and piercing holes. Its most significant advantage is that the material being cut is processed without interfering with its intrinsic structure as the heating of the material is very limited; (i.e. lack of thermal damage). Lower tool wear resulting from smaller cutting forces, enhanced fatigue strength characteristics, and higher productivity are other advantages. Romanowski et al.[5] investigated the influence of AWJ process parameters on the final part quality and presented a comparative analysis of the results with laser cutting. Moreover, Sutowska et al. [6] study the determination of the impact of curvature of a shape cut out in a brittle material (glass) using an AWJ. The AWJ cutting of a laminate is a complex phenomenon [7] due to the anisotropic nature of the material, the variation of the jet cutting forces, complexities due to nozzle diameter. The laminates under water jet cutting are exposed to different kinds of damages including matrix cracking, fiber pull-out, fiber roll-out, and delamination, which reduce their strengths and durability.

A few studies were performed previously to explain the underlying physics of the cutting of the composite structures subjected to AWJ. For instance, Ho-Cheng [8] reported that the interply damage occurred at the bottom surface of the composite because of the reduced strength of the uncut thickness as drilling depth increases. That increased the bending of the plies and causing delamination before the laminate was completely pierced. Shanmugam et al. [9] using a semi-empirical model, demonstrated that an increase in traverse speed led to an increase in the crack length due to the decreased abrasive dose, resulting in a poor cutting. The studies in [10,11] revealed that the interply damage could be decreased by increasing the kinetic energy of the AWJ while reducing the cutting speed. Hashish et al. [12] determined that the delamination could be decreased by reducing the diameter of the jet and supporting the material at the bottom. Colligan et al. [13] observed that there existed a critical traverse speed promoting the delamination. Schwartzenruber et al. [14] developed a one-way fluid–structure interaction (FSI) model to model the AWJ cutting. The transverse speed, abrasive flow rate, and mixing tube size were found to be responsible for the delamination. In another study [15], a transient two-way FSI model was developed to predict the delamination at the top ply when a CFRP laminate was exposed to the AWJ process. It was shown that the larger hydraulic shock loadings due to increased pressure and nozzle size led to an increase in the crack initiation and debonding. Li et al. [16] compared the hole quality and its impact on tensile behaviour of plain woven CFRP laminates subjected to pure water jet (PWJ) and AWJ cuttings experimentally. Recently, the study of Nyaboro et al. [17] demonstrated that the delamination was triggered by an increase in abrasive waterjet pressure and abrasive particle size, but was lessened by the rise in the standoff distance. The impact angle of the jet is one of the critical parameters affecting the process quality. In related studies, Junkar et al. [18] and Dadkhahipour et al. [19] showed its effect on the sphericity of craters for a stainless steel plate and the material removal process in AWJ milling of channels on an amorphous glass, respectively. On the other hand, intelligent algorithms including fuzzy logic systems [20–22] have been increasingly used to select optimal parameters in AJW cutting. A hybrid approach of fuzzy logic with genetic algorithm, an artificial neural network and regression model, the integration of vision-based monitoring and neuro-genetic control strategy were among the techniques used in this field. Vundavilli studied the performance of AWJ in terms of depth of cut, which relied on different process parameters, such as diameter of focusing nozzle, abrasive mass flow rate, water pressure and jet traverse speed [23].

However, the damage characteristics of the AWJ cutting of a cross-ply laminate are not described fully in the literature. For instance, progress of the damage along its thickness and at different interface layers, the sequence and interaction of different damage modes for various important process parameters need to be clarified. This will help us to understand the mechanics of the process; which, in turn, enables us to control and optimize the process in the industrial applications. This process was investigated here experimentally and numerically. In the performed tests, the pressure of AWJ particles and impact angle were varied. A three-dimensional FE model of the process was developed to understand the underlying physics. In the model, the abrasive and water jet particles were simulated using the smooth particle hydrodynamics. The 3D Hashin damage model [24] was used to simulate the failure behaviour of plies, and cohesive zone elements were used between plies to predict the delamination. The damage characteristics in the composite plate was investigated for different process parameters such as the impact angle and speed of the AWJ particles as well as the stacking sequence of the laminate in depth. The difference in the failure behaviour of the laminate subjected to AWJ and PWJ cuttings were highlighted.

2. Experimental investigation

In the AWJ cutting of laminates, different damage modes such as fibre breakage, fibre pull-out, delamination and matrix cracking were usually faced. Understanding their underlying reasons is important to optimise the manufacturing process and enhance the quality of the final product. To this end, firstly, an experimental investigation was performed. The used CFRP plates, manufactured by Volo Composite Solutions using unidirectional prepregs, were cured at a temperature of 180 °C and a pressure of 0.69 MP using a vacuum of 600 mm/Hg. Four layers were designed with a stacking sequence of [0°/90°/0°/90°], where its total thickness was 0.84 mm.

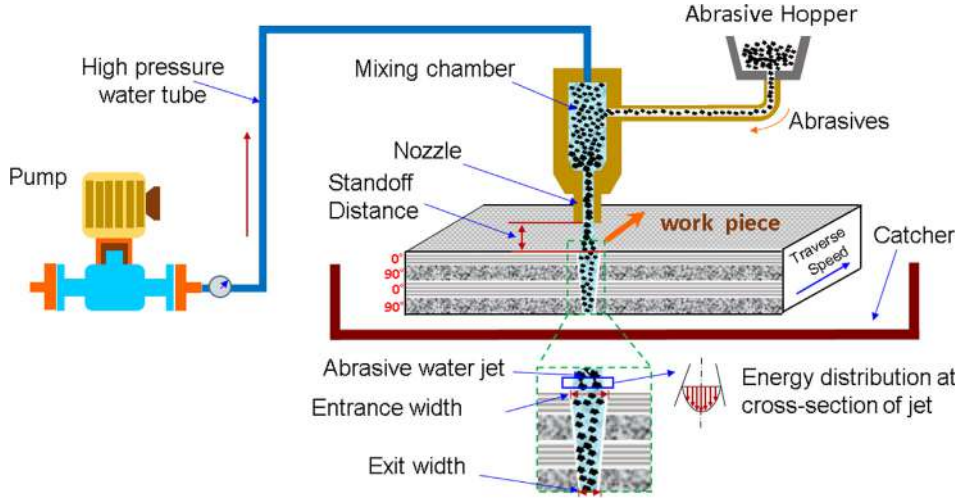

Fig. 1 Schematic diagram showing the characteristics of abrasive waterjet cutting.

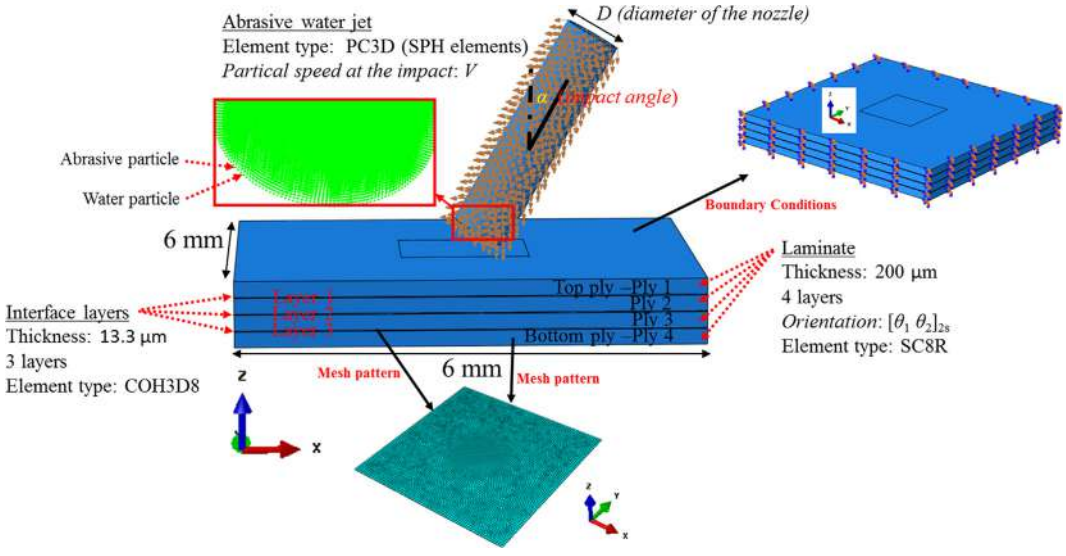

Fig. 2 Details of the developed 3D finite element model of the abrasive water jet cutting of the laminate.

The abrasive water jet machining using an abrasive mesh # 80 had a mean diameter 0.76 mm. Fig. 1 shows the principle of the conducted tests, where a high-pressure water supplied from the pump enters to the mixture chamber and is mixed with abrasive. The high-pressure abrasive water jet exits from the machine nozzle with specific parameters assuring the cutting process. The machine equipped with a CNC unit able to control the process parameters. In the tests, to invoke different damage modes in the composite plate, two different water pressures (200 and 400 MPa) and water jet impact angles (0° and 30°) were adjusted. To understand the damage characteristics of a CFRP laminate subjected to AWJ and state of the surfaces for different cutting parameters, the deformed samples were analysed using a scanning electron microscopy (SEM). The results obtained here will be presented and discussed in Section 4.

Table 1 Properties of abrasive and water particles [18,25,26].

Water	ρ (kg/m^3)	c_0 (m/s)	Dynamic viscosity (Pa.s)
	1000	1450	0.0011373
	s	Γ_0	
	0	0	
Abrasive	ρ (kg/m^3)	E (GPa)	Poisson's ratio
	4000	248	0.27

3. Numerical modelling of the water jet cutting

A three-dimensional FE model of the process was developed using ABAQUS 6.14 FE software. Fig. 2 presents its details. Dimensions of the sample used in the simulations were 6 mm × 6 mm × 0.84 mm. Eight-node continuum shell ele-

Table 2 Details of the material model used in the simulations [30].

	Equations [Condition]	Description of parameters
Intra-laminar damage initiation (Hashin Model)	$F_f^t = \left(\frac{\sigma_{11}}{X_T}\right)^2 + \left(\frac{\sigma_{12}}{S_L}\right)^2$ $[\sigma_{11} \geq 0]$ $F_f^C = \left(\frac{\sigma_{11}}{X_C}\right)^2$ $[\sigma_{11} < 0]$ $F_m^t = \left(\frac{\sigma_{22}}{Y_T}\right)^2 + \left(\frac{\sigma_{12}}{S_L}\right)^2$ $[\sigma_{22} \geq 0]$ $F_m^C = \left(\frac{\sigma_{22}}{2S_T}\right)^2 + \frac{\sigma_{22}}{Y_C}\left[\left(\frac{Y_C}{2S_T}\right)^2 - 1\right] + \frac{1}{(S_{12})^2}(\sigma_{12}^2)$ $[\sigma_{22} < 0]$	σ_{11}, σ_{22} = Stresses in the fiber and matrix directions, respectively σ_{12} = Shear stress X_T, X_C = The fiber tensile and the fiber compressive strengths, respectively Y_T, Y_C = The matrix tensile and the matrix compressive strengths, respectively S_L, S_T = The longitudinal and transversal shear strengths, respectively
Intra-laminar damage initiation	$d_I = \frac{\delta_{I,eq}^f(\delta_{I,eq} - \delta_{I,eq}^0)}{\delta_{I,eq}(\delta_{I,eq}^f - \delta_{I,eq}^0)}$ $(I = ft, fc, mt, mc)$ $\delta_{I,eq}^f = 2G_I/\sigma_{I,eq}$ $d_s = 1 - (1 - d_{ft})*$ $(1 - d_{fc}) * (1 - d_{mt}) * (1 - d_{mc})$	d_I = The degradation (damage) coefficient for different modes (I) ft , fc = fiber tension and compression mt , mc = matrix tension and compression $\sigma_{I,eq}$ = The equivalent stress $\delta_{I,eq}^0$ = The equivalent stress at the onset of damage $\delta_{I,eq}$ = The equivalent displacement $\delta_{I,eq}^0$ = The equivalent displacement at the onset of damage G_I = The fracture toughness of the material d_s = The shear damage
Onset of delamination	Quadratic nominal stress criterion $\left(\frac{\langle T_1 \rangle}{T_1^0}\right)^2 + \left(\frac{T_2}{T_2^0}\right)^2 + \left(\frac{T_3}{T_3^0}\right)^2 = 1$ $\langle \cdot \rangle$ is the Macaulay bracket QuadScrt = The Quadratic Nominal Stress Criterion considers a combination between the nominal stress (T_i, i) and the allowable stress acting in different directions (T_i^0, i),$0 \leq$ QuadScrt ≤ 1	T_i = Tractions for each pure mode i T_i^0 = Interfacial normal and shear strength values for each pure mode i Pure normal mode (i = 1) First (i = 2) and second (i = 3) shear directions
Propagation of delamination	Power law criterion $\left(\frac{G_1}{G_1^0}\right)^2 + \left(\frac{G_2}{G_2^0}\right)^2 + \left(\frac{G_3}{G_3^0}\right)^2 = 1$ $\delta_c = 2G_c/\delta_0 E_0$ SDEG = It represents the state of damage in an element, $0(\text{nodamage}) \leq \text{SDEG} \leq 1(\text{completedamage})$	G_i = The Energy Release Rate for each pure mode i G_i^0 = The Critical Energy Release Rate for each pure mode i δ_0 : The value of mixed-mode separation at damage initiation E_0: Penalty stiffness - initial slope of the bilinear curve

ments with reduced integration (SC8R) were used to discretize the laminate volume. The delamination, i.e. the interlaminar damage, was taken into account in the simulations using 8-node three-dimensional cohesive elements (COH3D8) with a thickness of approx. 13 μm. Based on the mesh convergency study considering the von Mises stress on the composite plies, an element size of 60 nm in the longitudinal and transverse directions was used at the centre of the sample, and a coarser mesh was used elsewhere. An identical mesh pattern was used for the interface layers. Tie constraints were defined between the composite plies and the interface layers.

The mixture of abrasive and water particles with an impact angle of α is simulated as a cylinder with a diameter of 0.76 mm and a length of 10 mm. They were meshed using Smoothed particle hydrodynamics (SPH) elements with a type of PC3D. The distance between two particles is 7.5 μm. Node sets were created using the mesh to predefine the speed (V) of particles. The arrows in Fig. 2 are the components of the velocity vector. As the impact time was very short (a run time of 0.5×10^{-6} s was considered in the simulations), the heat exchange and vaporization of water were not considered. The water particles were modelled using the linear Hugoniot form of the Mie-Grüneisen equation of state (EOS). It is a relation between the pressure and the volume of a material at a given temperature [25]. ABAQUS/Explicit provides a linear U_s–U_p equation of state model that can simulate incompressible viscous and inviscid laminar flow governed by the Navier-Stokes Equation of Motion [26]. The linear U_s–U_p Hugoniot form can be written as follows

$$p = \frac{\rho_0 c_0^2 \eta}{(1 - s\eta)^2}\left(1 - \frac{\Gamma_0 \eta}{2}\right) + \Gamma_0 \rho_0 E_m \quad (1)$$

where p is the pressure stress, ρ_0 and ρ are the reference density and current mass density, respectively, c_0 (speed of sound), s and Γ_0 are material constants defining the linear relationship between the linear shock velocity U_s and the particle velocity U_p as $U_s = c_0 + sU_p$, η is the nominal volumetric compressive strain and equal to 1-ρ_0/ρ and E_m is the internal energy per unit mass. The properties of water and highly rigid abrasive jet particles considered in the simulations are shown in Table 1.

The boundary conditions for the specimen were as follows: Since the plate was not bendable, its sides was set to be restrained in all directions so that the plate could not move in any direction following the study in [27]. An explicit time integration scheme was selected for this process. A general contact algorithm was used to define the interaction between the water jet and the composite workpiece. The interaction properties were set to hard contact for the normal behaviour and frictionless contact for the tangential behaviour following the study [28].

A 3D Hashin's failure criterion, a continuum damage model, was adopted to model intralaminar damage considering fibre breakage and matrix cracking. In this model, the onset of degradation occurs when the maximum value of the equivalent stress limit was reached, beyond which damage started to propagate; the material behaves elastically before any of the failure criteria was satisfied. On the other hand, the inter-laminar damage including its onset and evolution was simulated by adopting the Cohesive Zone Method (CZM) [29]. Table 2 summarizes the constitutive equations used in the simulation of intra-laminar and inter-laminar damages. The elements were deleted from the simulations when the complete damage was reached for both damage models. The material constants including the damage parameter used in the simulations are shown in Table 3. The simulations run an average of 9 h on the HPC cluster of 32 CPUs (Intel(R) Xeon(R) CPU E5 − 2630 v3 @ 2.40 GHz).

4. Results and discussions

4.1. Experimental observations

Fig. 3-a illustrates the damage characteristics in the cross-section surface obtained by the AWJ process with a water pressure of 200 MPa and the impact occurred perpendicular to the composite sample ($\alpha = 0°$). A substantial delamination was developed between the layers within the cohesive zone. The fibers in the ply with 90° orientation were subjected to shearing loading. Moreover, localized damage was observed due to the micro impact of abrasive particles on the fractured surface. The fibers breakage and pull-outs phenomena were observed

Table 3 Material properties used in the finite element model [30,31].

	Density (kg/m^3)/Elastic (MPa)					
Intra-ply	Density	E_{11}	$E_{22} = E_{33}$	ϑ_{12}	$G_{12} = G_{13}$	G_{23}
	1780	122,000	6200	0.35	4400	3700
Inter-ply	Density	K (GPa/mm)				
	1780	300				
	Strength (MPa)					
Intra-ply	σ_{1T}^u	σ_{1C}^u	σ_{2T}^u	σ_{2C}^u	σ_{12}^u, σ_{13}^u	σ_{23}^u
	1850	1470	29	290	65	65
Inter-ply	T_1^0	T_2^0	T_3^0			
	30	80	80			
	Damage (kJ/m^2)					
Intra-ply	G_{ft}	G_{fc}	G_{mt}	G_{mc}		
	92	80	0.52	1.61		
Inter-ply	G_1^0	G_2^0	G_3^0			
	0.52	0.92	0.92			

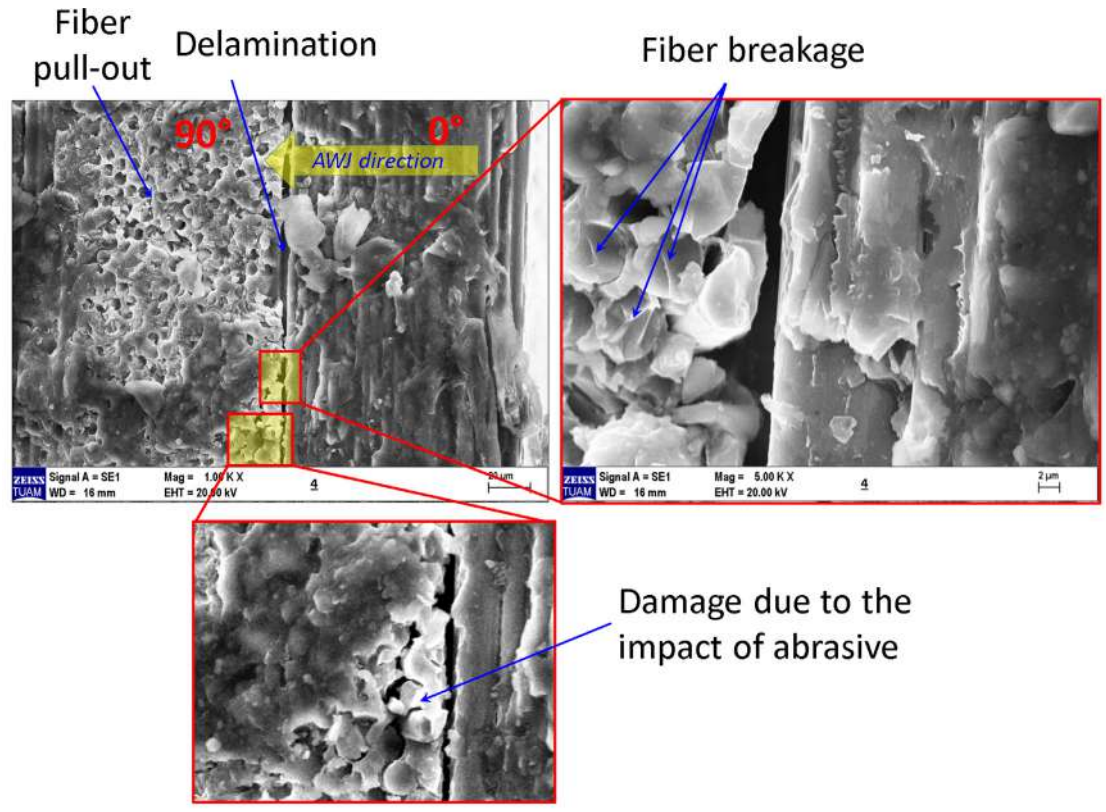

Fig. 3 SEM micrographs of AWJ perpendicular to CFRP plate with water pressure of (a) 200 MPa, (b) 400 MPa.

in this layer. In the ply with fibers oriented with 0°, the damage was obviously observed in the matrix and the fibres were separated smoothly without breakage within the fracture plane. Fig. 3-b shows important changes in the damage characteristics of CFRP machined surface due to the increase of AWJ pressure from 200 to 400 MPa. A substantial debonding of the fibers and fiber breakage were observed in the layer with fibers oriented 0°, consequently the imprint of these damaged fibers caused a poor surface quality. Moreover, fibers pull-out was observed in the layer with fibers 90° but with less frequency compared to those at lower pressure (200 Mpa). Fig. 4 shows the results of SEM observation for the case of AWJ oriented with 30° impact angle and pressure 400 MPa. This configuration favoured abrasive particles to embed between plies

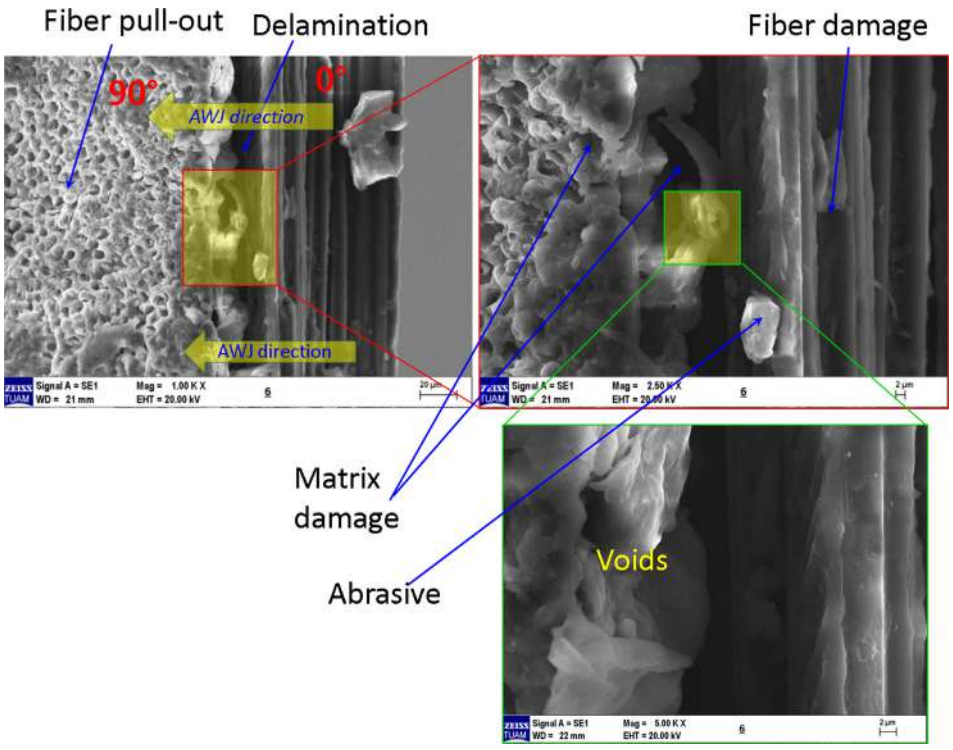

Fig. 4 SEM micrographs of machined CFRP plate subjected to AWJ with $\alpha = 30°$ and water pressure of 400 MPa.

Table 4 Process parameters setup in FE simulations (plan of simulations).

Speed of water jet (m/s)	Orientation of the laminate	Type of particles	Impact angle (°)
600	0°/90°/0°/90°	AWJ	0
480	0°/90°/90°/0°	PWJ	15
300	0°/0°/90°/90°		30

and in the damaged matrix, significantly contributing to develop discontinuities between layers in the cohesive zone. This AWJ configuration was susceptible to a complicated failure pattern with a combination of matrix damage, delamination, burr with fibers cut and fibers pull-out. The inclined attack of AWJ particles did not lead to a pure shearing of the fibers but instead led to fiber pull-out mostly in the second ply where the fibers were oriented 90°.

4.2. Numerical observations

The experimental observations done in Section 4.1 demonstrated that the AWJ cutting of a laminate was quite complicated, where different damage modes took place in the deformed cross-section concurrently. To detect onset and progress of each damage mode, their sequence and interactions as well as how they propagated along the thickness of the laminate, a detailed numerical analysis was performed for different process parameters. In this section, the varied parameters are speed of water jet, stacking sequence of the laminate, type of impacting particles, and impact angle. For each of them, two or three different cases were considered as shown in Table 4. In the reference model, the abrasive particles accompanied with water jet particles penetrated the [0/90/0/90] laminate with an impact angle of 0° and had an impact speed of 480 m/s.

Fig. 5 presents the distributions of different failure modes on the cross-section of the laminate at 0.500 μs. It was observed that the damage in the fibers started only at the top ply, where both tensile (*ft*) and compression (*fc*) modes were activated. A similar observation could be made for the matrix compression damage (*mc*), where the plies did not experience any amount of this damage except the top one. However, an extended tensile matrix cracking (*mt*) along the thickness of the plate was observed. It was concluded that while both of the fiber failure modes and matrix compression failure were localized only at the top ply, matrix tensile failure mode was prevalent in the composite laminate.

Fig. 6 presents the distributions of matrix tensile cracking and delamination failure at different time instants obtained using the reference model. The first frame at 0.100 μs after the initial contact between the water jet particles and the composite plate shows a matrix failure at the upper part of the top ply only, whereas no interply failure was observed. With an advancement of the abrasive and water jet particles towards laminate ($t = 0.200$ μs), the tensile matrix damage reached the limits of the top ply and the top interface layer started experiencing damage. At $t = 0.300$ μs, while the matrix damage covered the second upper ply, the delamination was observed at the top interface and the cohesive damage was experienced in the second interface [30]. At $t = 0.400$ μs and $t = 0.500$ μs, both damages continued to spread in the thick-

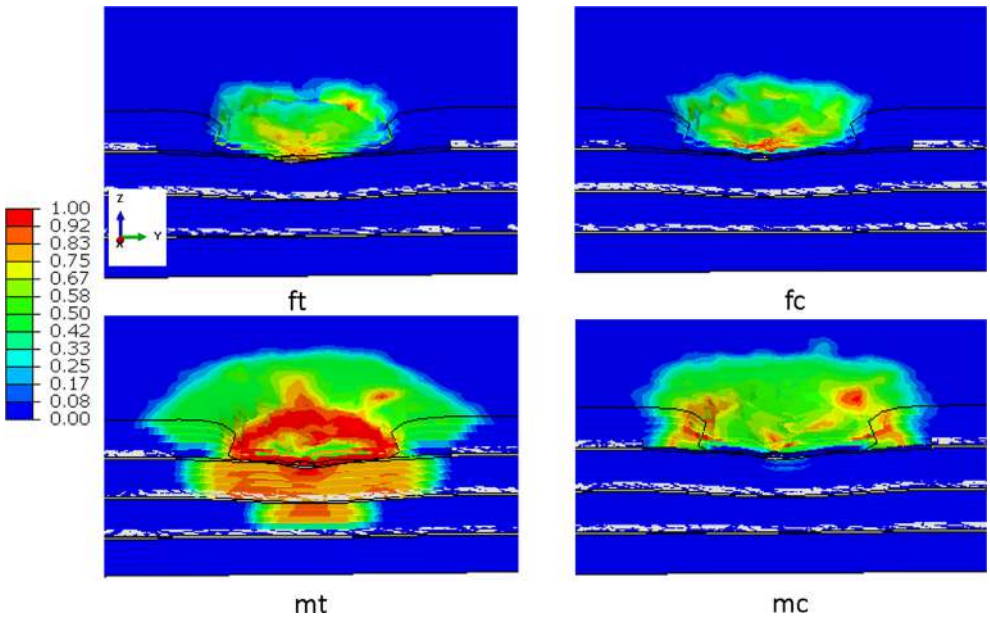

Fig. 5 Distributions of different fiber and matrix damages in the composite plate at 0.500 μs.

ness direction similar to earlier time instants. As a result, all the plies except the bottom one and all the interfaces experienced matrix cracking and cohesive damage, respectively. However, the delamination was observed only between the two top plies. The amount of delamination was quantified as the ratio of the number of elements deleted to the total number of elements existing in the layer at the beginning of the process, in %. The amount of delamination increased from 4.02% to 6.00% from $t = 0.300$ μs to $t = 0.500$ μs. Obviously, with the progression of the matrix cracking in the thickness direction, the cohesive damage was triggered. Since the fiber damage was localized at the top lamina only at the beginning of cutting, it was concluded that the matrix failure, essentially its tensile mode, triggered the delamination in the composite plate when subjected to the water jet cutting.

4.2.1. Influence of water jet speed

In this part, the influence of the speed of abrasive water jet particles on the progress of damage in the laminate was investigated. Three different values of V, 600 m/s, 480 m/s and 300 m/s, were considered. Fig. 7 presents the respective distribution of tensile matrix damage in the composite plate. The results were presented at different time instants, namely 0.400 μs, 0.500 μs, and 0.600 μs to keep the distance of the particles traveled constant with the value of 0.24 mm for all the configurations. It was noticed that with a decrease in the speed of the particles, the tensile matrix damage propagated more in the impact direction. For instance, it hardly reached the third ply for V equalled to 600 m/s, it not only reached the bottom lamina but also became prominent there for V equalled to 300 m/s.

Fig. 8 presents the distribution of cohesive damage with the amount of delamination on different interface layers for different speeds. At the top interface layer, the amount of delamination increased from 5.69% to 6.00% and 6.44% when V decreased from 600 m/s to 480 m/s and later to 300 m/s. A similar trend was noticed for the middle and bottom interfaces, where the spread of cohesive damage increased for lower cutting speeds. While no delamination was observed for the respective layers for $V = 600$ m/s and 480 m/s, it existed for the lowest speed. As expected, no cohesive damage was observed at the bottom interface layer for $V = 600$ m/s since the matrix cracking did not develop at the bottom ply as seen in Fig. 9; thus, the interface damage was not triggered. The amount of delamination was highest with 6.44% at the top interface followed by 2.86% at the bottom and 1.74% at the middle one for $V = 300$ m/s. Our findings here complied with the experimental result in Wong et al. [10]. It was demonstrated that for higher hydraulic pressure, i.e. higher particle speeds, the abrasive particles maintained their kinetic energy to cut through the composite laminate progressively. That produced a small degree of bending fractures of the fibre and gave a clean kerf border with less delamination damage.

The propagation of delamination is governed by the shear stress variation across the laminate thickness. In connection with this, to explain the difference in the delamination characteristics for different speeds, the shear deformation in the composite plies was investigated. Fig. 9 shows the distributions of shear damage on the faces of the plies adjacent to the interface layers for $V = 600$ m/s and 300 m/s. For instance, to describe the delamination in Layer 2, the damage on the bottom face of Ply 2 and the top surface of Ply 3 as the adjacent faces were analyzed. The regions with grey and blue colours represent the areas with and without shear damage, respectively. It was observed that the shear damage on the bottom surface of the top ply and the upper surface of the second ply for $V = 600$ m/s were less than those for $V = 300$ m/s. This explains why the delamination area was larger for the latter with 6.44% when compared to the former with 5.69%. Even though the values of shear damage on the faces of the plies contacting the middle and bottom interface layer were not so different from each other for V equalled to 300 m/s, the delamination areas, 1.74% and 2.86%, respectively, were not close. However, it should be noted that the areas exposed to cohesive damage shown in Fig. 8, the non-blue region, were very close to each other for the second and third interface layers.

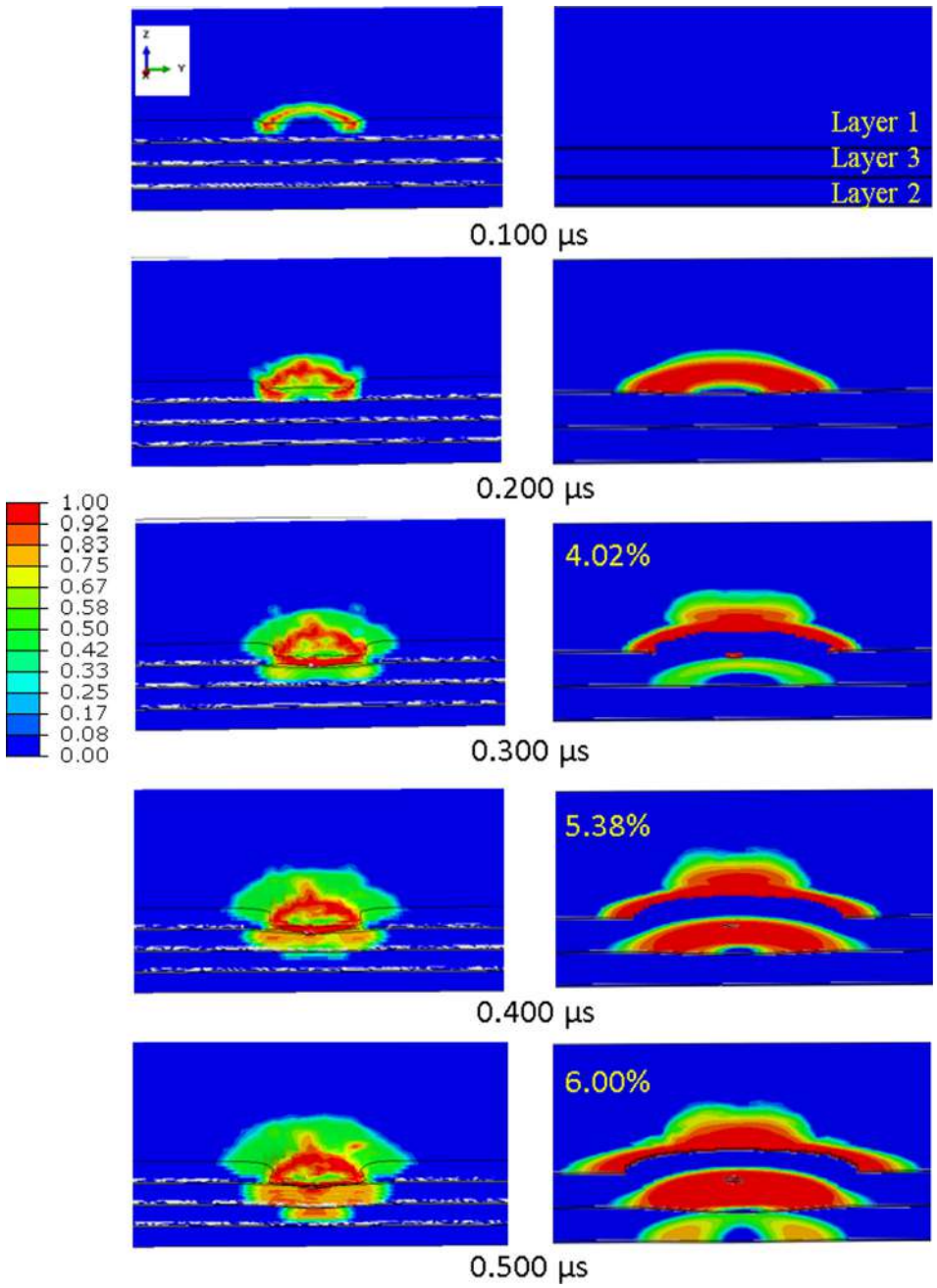

Fig. 6 Evolution of the matrix tensile damage in the composite plate with the propagation of the delamination at different interfaces including its amount in%.

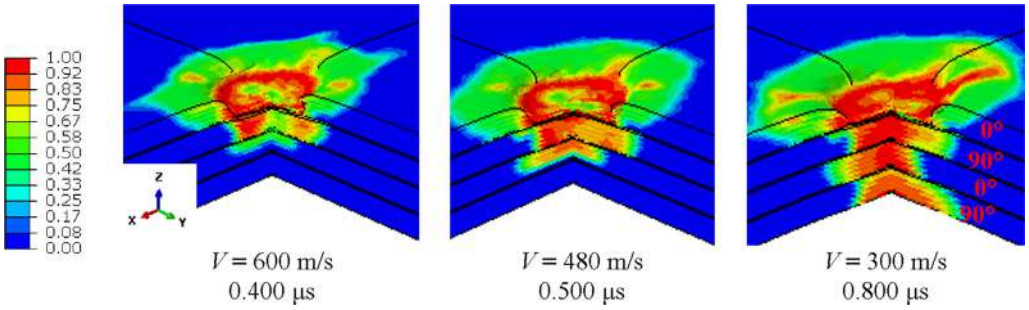

Fig. 7 Distributions of tensile matrix damage in the composite plate for different speeds of cutting particles.

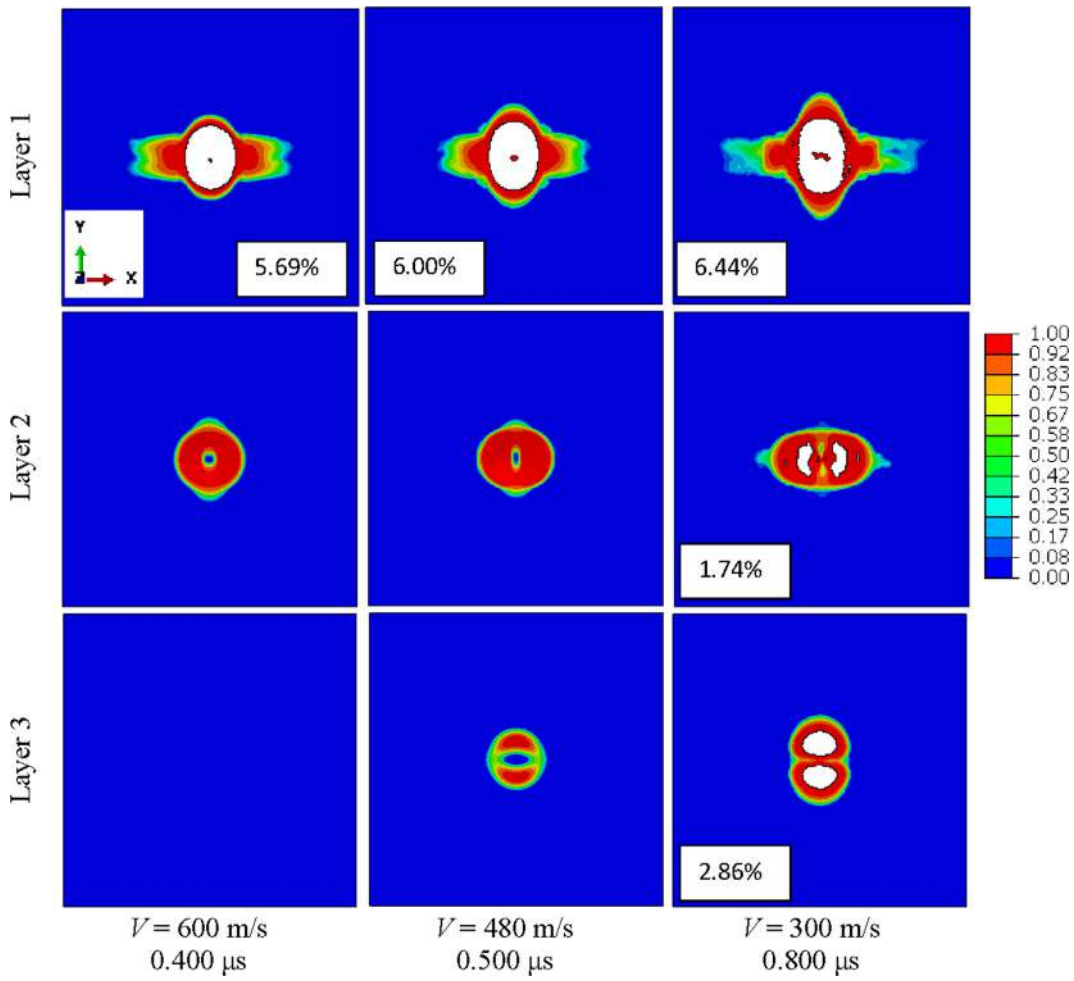

Fig. 8 Degradations of the cohesive elements including the areas delaminated (with their amounts in%) at different interfaces of the composite plate for different speeds of cutting particles.

Fig. 10 compares the area of the top ply exposed to fiber damage for the cases investigated here. As noticed, with a decrease in V, a smaller area experienced fiber tension and fiber compression damages. It was concluded that with an increase in speed of particles, the deformation was confined to the top plies only resulted in both fiber and matrix damages there while the matrix cracking and the delamination at the bottom plies and interface layers, respectively, became less possible. This complies with the experimental microscopic analysis presented in Fig. 3, where the fiber damage was more significant for higher pressure of the AWJ.

4.2.2. Influence of the orientation of the laminate

In this section, three different orientations, 0°/90°/0°/90°, 0°/90°/90°/0° and 0°/0°/90°/90°, were considered to investigate the influence of stacking sequence on the deformation response of the laminate under abrasive water jet cutting. A few studies [32,33] showed that the interface between two adjacent plies having the same orientation angle such as 0°/0° or 90°/90° did not lead to delamination. Thus, such interfaces were not modelled here. Therefore, there existed only 2 and 1 interfaces for the second and third orientations studied here, respectively. The distribution of tensile matrix damage presented in Fig. 11 showed that some differences were noticed when the laminate orientation was changed. While the matrix cracking was severe only in the top two plies and limited amount in the third ply for 0°/90°/0°/90°, it was significant for all the plies except the bottommost one for 0°/90°/90°/0°, where it was negligibly small for this 0° ply. On the other hand, all the plies experienced significant matrix damage for 0°/0°/90°/90°. This observation can be evaluated considering the interface layers between the plies having different orientations. As the number of layers was less with 2 and 1 for the second and third orientations, respectively, the matrix cracking propagates more in the impact direction when compared to the first orientation with three interface layers. It can be concluded that the interface layers act as obstacles to the spread of the matrix damage in the thickness direction.

Damage of the cohesive elements at the interfaces was also analyzed (see Fig. 12). They were compared for the first two orientations. While the cohesive damage on the top interface layers as close to each other with delamination amounts of 6.00% and 6.65%, it was more significant on the bottom interface for the second orientation when compared to the first one. On the other hand, the area exposed to cohesive damage and delamination was largest at the interface, being the only existing layer, for the third orientation considering the other stacking sequences. Here we concluded that when the number of

cohesive layers decreased, the interface layers had to sustain more loads themselves; thus, they were exposed to more damage and delamination became more prominent.

4.2.3. *Influence of the abrasive particles*

In this section, the influence of abrasive particles in cutting the laminate was investigated. For this purpose, the damage patterns obtained with the reference model using the abrasive water jet (AWJ) cutting were compared with those obtained using the pure water jet (PWJ) cutting. In the latter, the abrasive particles were replaced with the water particles. Fig. 13 presents the distributions of *fc*, *ft* damages on the upper surface of the composite and *mt* damage on the upper surface as well as at the cross-section obtained using both cutting techniques. Damage of the fibers either tensile or compressive looks similar for both AWJ and PWJ. However, they spread to a larger area for the former one compared to the latter, especially for the fiber compression mode. Specifically, the diago-

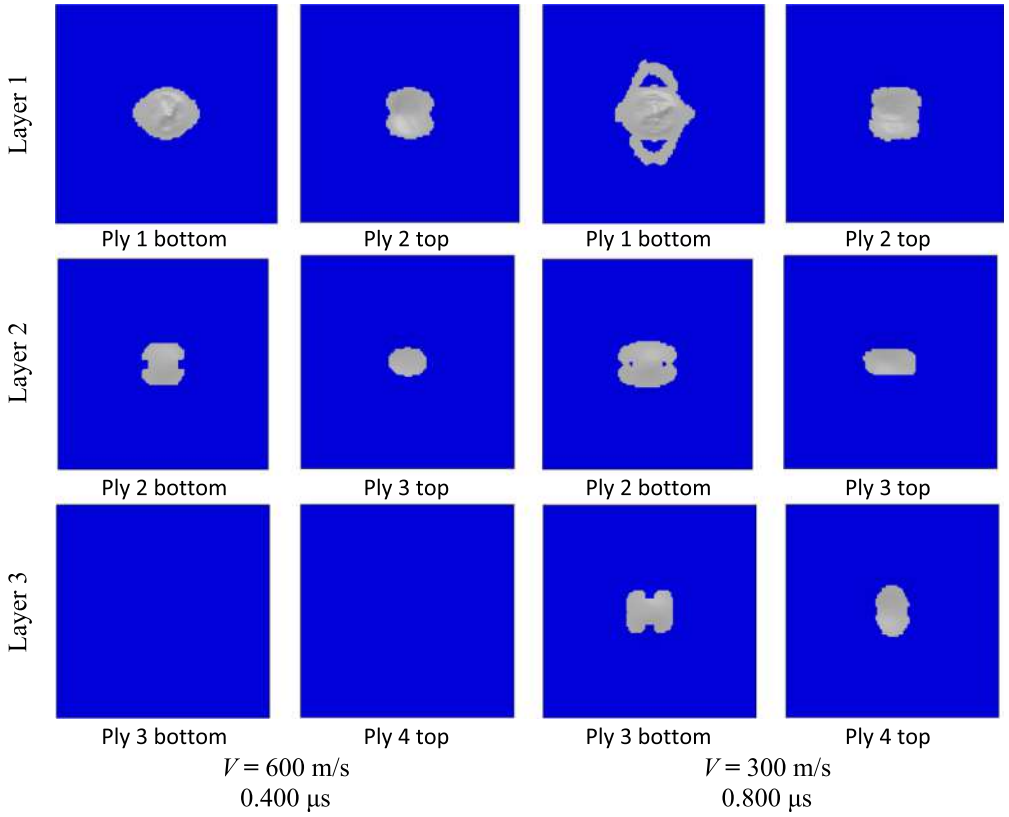

Fig. 9 Distributions of shear damage on the surfaces of the plies in contact with the interface layers for V equals to 600 m/s and 300 m/s.

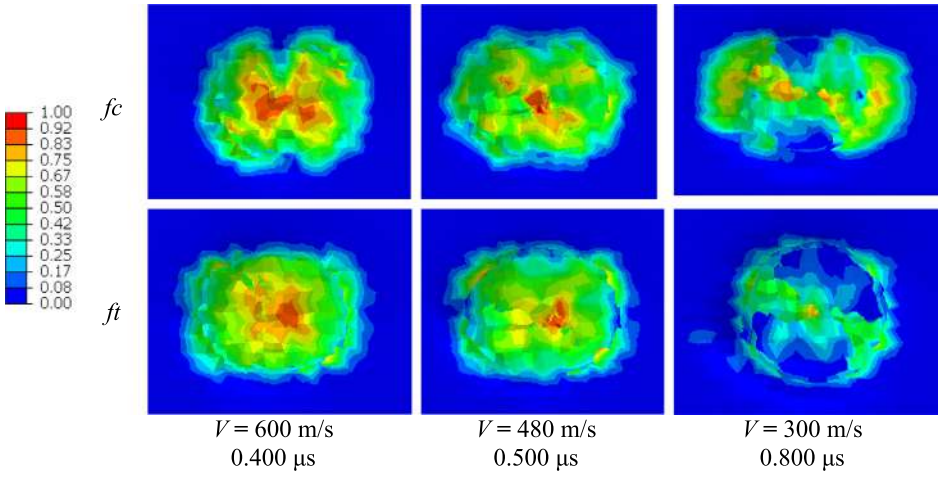

Fig. 10 Distributions of fiber compression (*fc*) and fiber tension (*ft*) damages on the upper surfaces of the topmost plies for different speeds of particles.

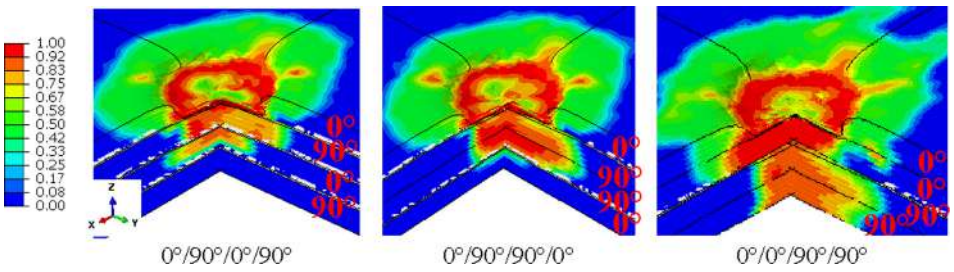

Fig. 11 Distributions of matrix tensile damage at the cross-sections of the composite plates with different orientations at 0.500 μs.

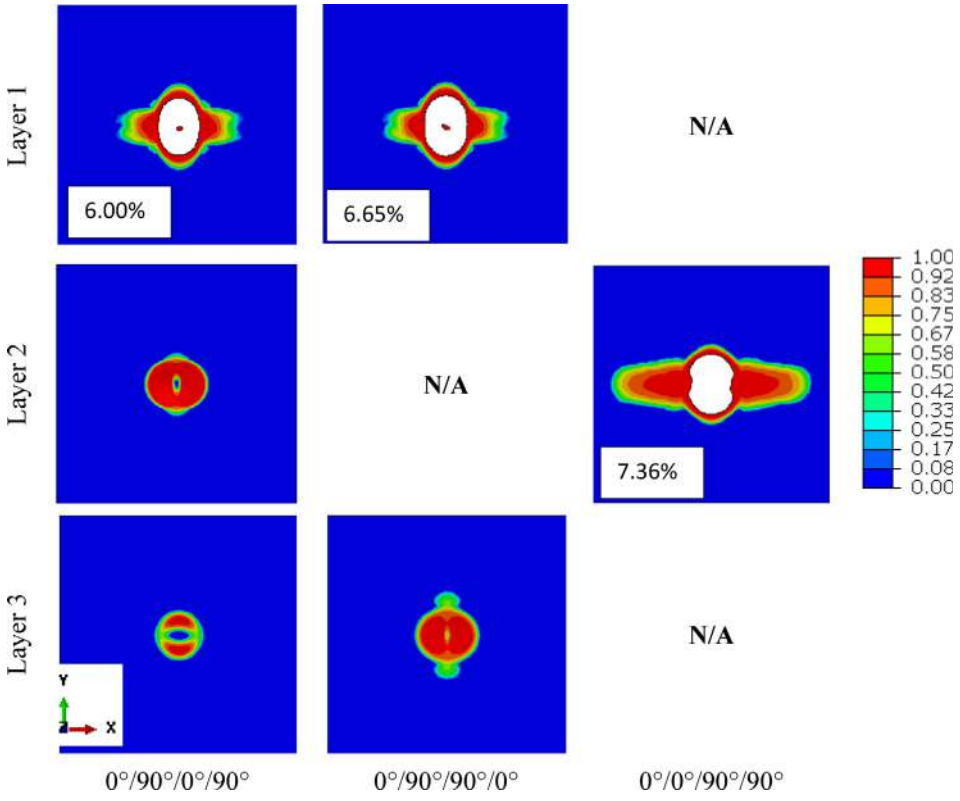

Fig. 12 Degradations of the cohesive elements including the areas delaminated (with their amounts in%) at different interfaces of the laminates with different stacking sequences at 0.500 μs.

nal length of the damaged area due to fiber compression was 1.18 mm and 1.02 mm for the AWJ and PWJ, respectively. For the fiber tension damage mode, they were 1.10 mm and 1.01 mm, respectively. On the other hand, the distribution of tensile matrix cracking was not affected by the cutting type significantly. That is also reflected in Fig. 14, where the damage progress at the interface layers was shown. They were very similar to each other for AWJ and PWJ. Only, the amount of delamination was at the topmost layer for PWJ (5.13%) was slightly smaller than that for AWJ (6.00%). That was due to less amount of matrix tensile damage on the second upper ply when pure water jet particles were used for the cutting instead of the abrasive particles.

To evaluate the cutting performance of AWJ and PWJ, the roughness of the uppermost ply surface was compared. Fig. 15 demonstrates the distribution of the displacement in the z-direction at the mentioned surface. They were the bottom-up perspective views. It is clear that the gradients of the displacement values are steeper when the PWJ cutting was used. That can also be seen from Fig. 16, where the displacements in the z-direction, larger than 0.15 mm, for different material points were plotted. Obviously, that a smoother surface is obtained when the PWJ cutting is used as much more material points experience deformation of the particles equally rather than differently as in the AWJ. In other words, a more valley type of deformed surface was obtained when the PWJ was used; whereas, a conical deformed surface was attained using the AWJ cutting. Consequently, when the abrasive particles accompanied by water particles were used to cut the laminate instead of the pure water jet particles, the cutting was realized more efficiently as more fibers were damaged; whereas, its delamination characteristics did not change sensibly. The findings here complied with those reported in [16]. It was revealed that the abrasives in waterjet cutting enhanced surface integ-

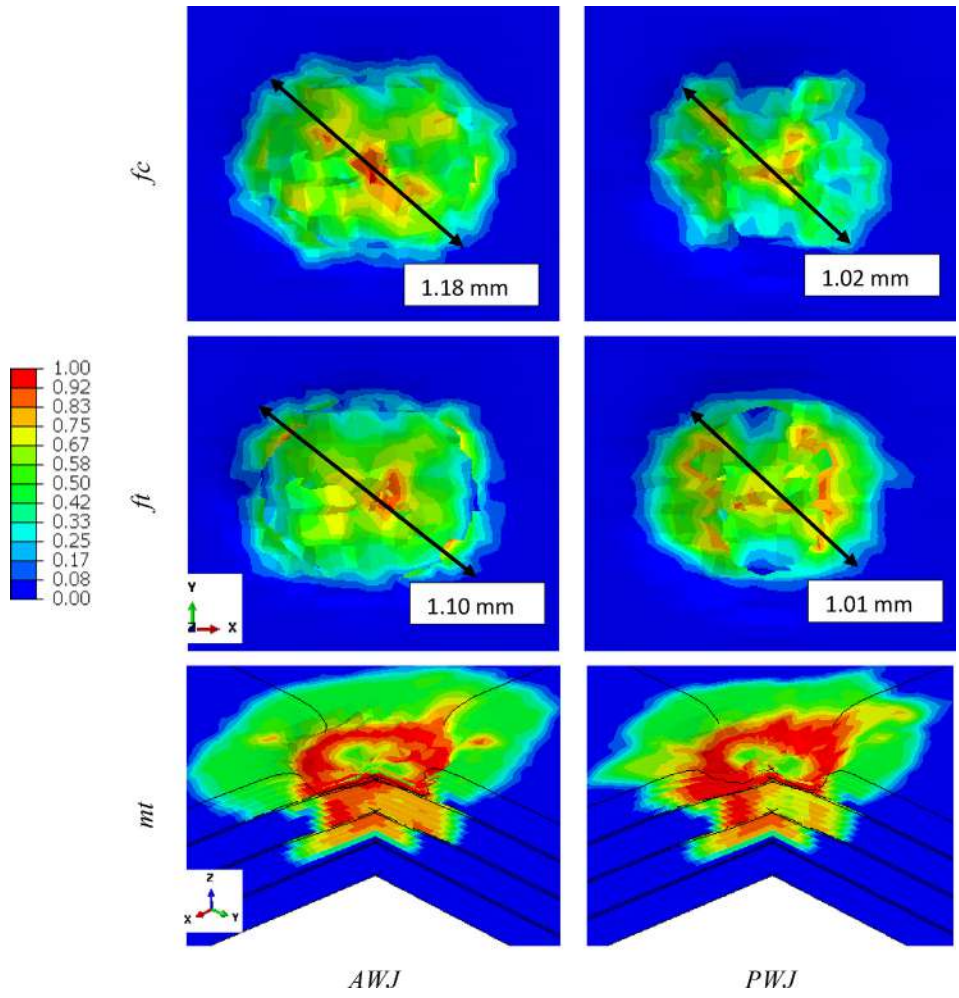

Fig. 13 Distributions of fiber compression (*fc*) and fiber tension (*ft*) damages on the upper surfaces of the topmost plies as well as the matrix tensile (*mt*) damage at the cross-sections of the composite plates being cut using different techniques at 0.500 μs.

rity significantly, and massive delamination, fiber breakage, and splitting bounds were the main features for both AWJ and PWJ.

4.2.4. Influence of impact angle

In this last part, the response of the composite laminate for three different impact angles of water jet particles, i.e. $\alpha = 0°$, 15° and 30°, are investigated. Fig. 17 presents the distribution of tensile matrix damage on different plies and the cohesive damage at the interfaces at 0.500 μs. It was observed that with an increase in α, the amount of penetration on the surface of the laminate decreased substantially, while the amount of matrix cracking and its spread decreased noticeably. In parallel, the degradation of the cohesive elements on different interfaces of the composite plate decreased with an increase in α. For instance, the amount of delamination at the top interface was 1.10% and 2.92% only when $\alpha = 30°$ and 15°, respectively. Considering the respective value for $\alpha = 0°$, 6.0%, the quantity of delamination dropped significantly. Since the matrix cracking reached second bottom lamina for $\alpha = 15°$, the middle interface experienced cohesive damage. However, the interface damage was restricted to the top interface layer only for $\alpha = 30°$, because the matrix damage was confined to top two plies only. The material removal rate - as a result of the cutting of fibers - and depth of cut were increased when the cutting occurred without inclination of the particles [19]. A direct comparison of the numerical findings here with those of the experiments may not be correct as the former simulates the very beginning of the AWJ process; whereas, the experimental microscopic analyses were done in the specimens after the cutting process was completed.

5. Conclusion

In this study, a 3D FE model of the abrasive water jet cutting of a cross-ply CFRP laminate was developed to describe the experimentally observed damage characteristics at the onset of AWJ cutting process. The smooth particle hydrodynamics was used to simulate the water jet and abrasive jet particles. The intraply and interply damage in the laminate were simulated using 3D Hashin damage model and cohesive zone model, respectively.

From this study, the following conclusions were drawn:

- When the abrasive water jet particles started cutting the laminate, the matrix cracking in tensile mode was triggered initially, which, in turn, led the delamination to start from

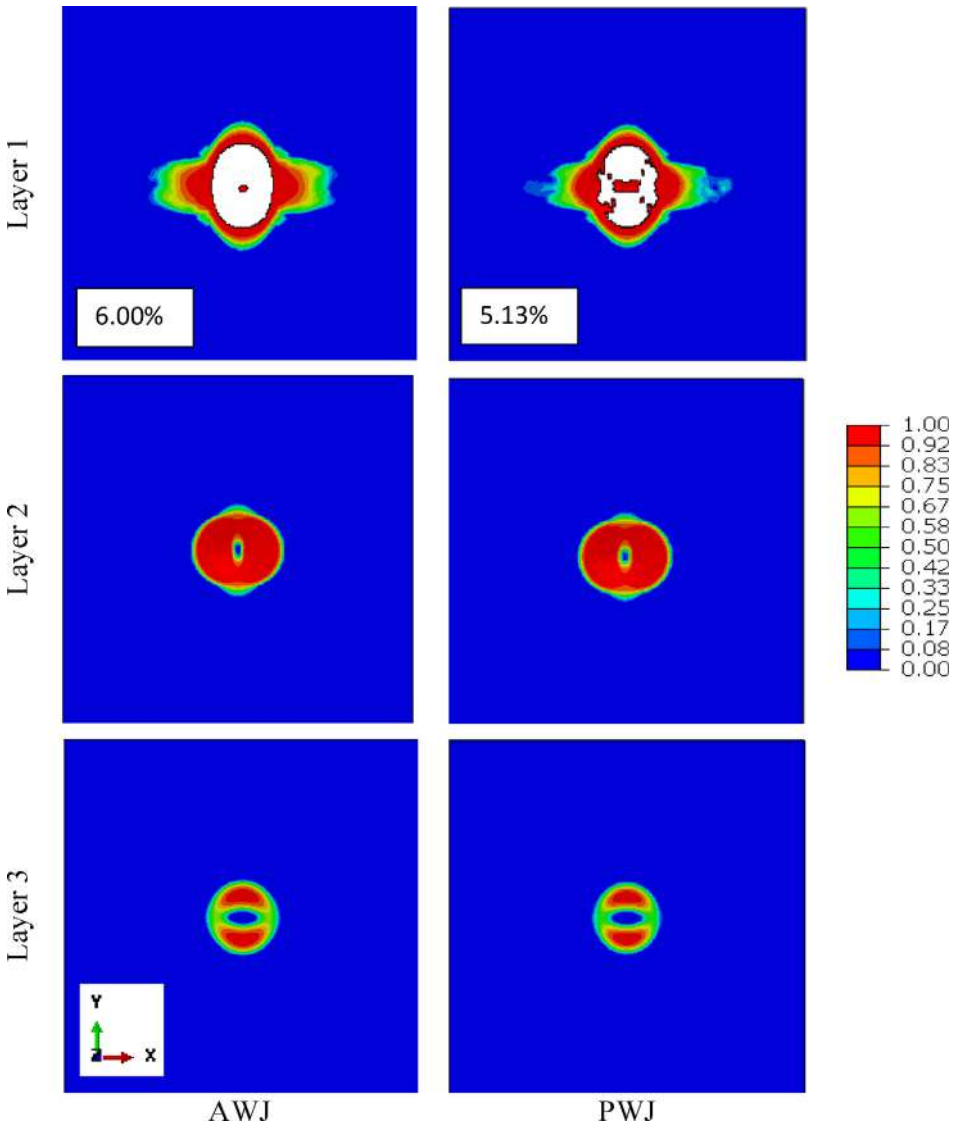

Fig. 14 Degradations of the cohesive elements including the areas delaminated (with their amounts in%) at different interfaces of the laminates being cut using different techniques at 0.500 μs.

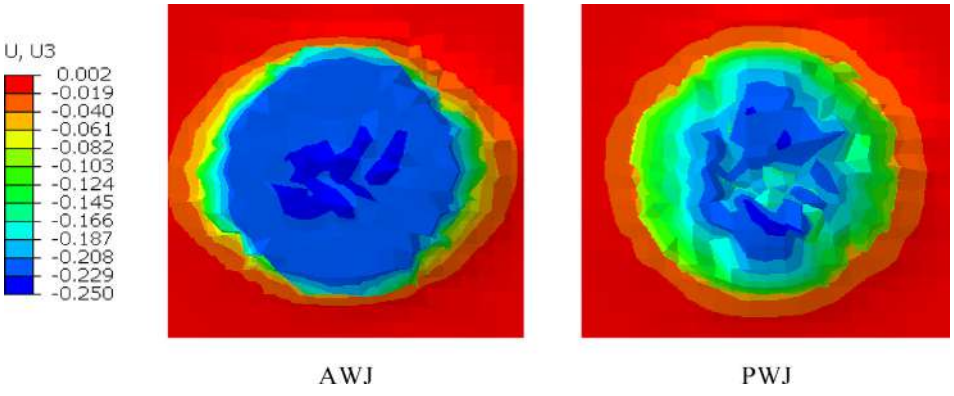

Fig. 15 Distributions of displacement in z-direction on the upper surface of the topmost ply of the composite plate (bottom up perspective views) being cut using different techniques at 0.500 μs.

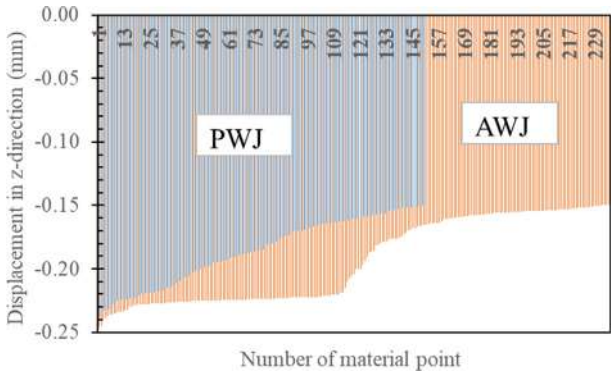

Fig. 16 Number of material points on the upper surface of the topmost ply having the displacements in the z-direction larger than 0.15 mm for PWJ and AWJ processes.

the topmost interface layer to the lower ones in a row. In parallel, the damage in the fibers was restricted to the upmost ply only.

- In the case of AWJ with lower cutting speed of the particles, the intraply and interply damages were more distributed along the thickness of the laminate, i.e. the matrix cracking and delamination became more prominent at the lower plies and the lower interface layers, respectively. However, the fiber damage at the top ply became less significant. This is in line with the experimental observation, where the fiber damage became less significant for lower pressure of the AWJ.
- The orientation of the cross-plied laminate exposed to AWJ affects the propagation of the cracks, where the interface layers act as obstacles to the spread of the matrix damage in the thickness direction.
- The abrasive particles in AWJ let the cutting process realize more efficiently, where a smoother cutting occurs via the fibers were cut properly when compared to the PWJ. However, the characteristics of interlaminar damage did not change a lot.
- With an increase in impact angle, the abrasive particles could not penetrate the laminate easily; thus the cutting became difficult. The experimental analysis demonstrated that the fiber pull-out in the ply with 90° became more prominent for larger impact angles.

The findings in this study can be used for an adequate estimation of the AWJ cutting performance of laminates and might be used for process control as well as optimizing the process parameters. In the future, the numerical model will be advanced for a coupled analysis of FEM and Computational Fluid Dynamics (CFD), where the CFD domain was first solved and the pressure loads were exported to the structural domain for the damage analysis.

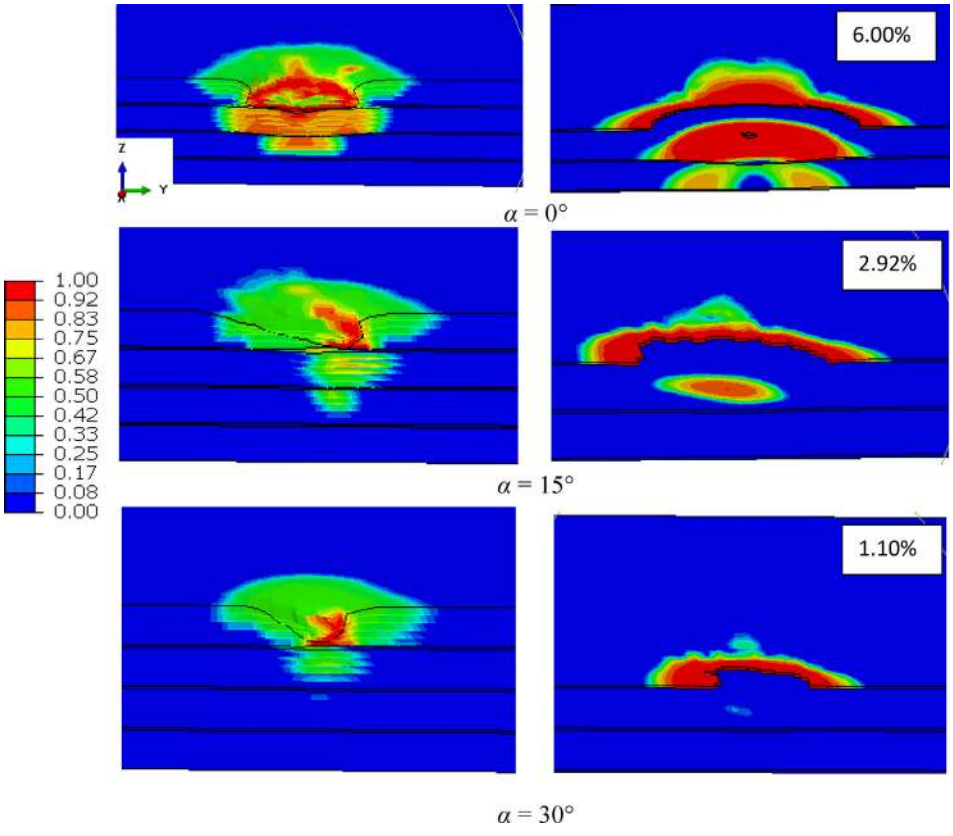

Fig. 17 Distributions of the matrix tensile damage at the cross sections including the areas delaminated (with their amounts in%) at different interfaces of the composite plates for different impact angles of particles at 0.500 μs.

Declaration of Competing Interest

The authors declare that they have no known competing financial interests or personal relationships that could have appeared to influence the work reported in this paper.

References

[1] F. Ahmad, H. Mehboob, F. Abbassi, J.-W. Hong, J. Zghal, A. Mehboob, Numerical investigation to evaluate the energy effect on the impact resistance of an aircraft carbon fiber-reinforced polymer composite, Mech. Adv. Mater. Struct. (2021) 1–11.
[2] F. Abbassi, I. Elfaleh, S. Mistou, A. Zghal, M. Fazzini, T. Djilali, Experimental and numerical investigations of a thermoplastic composite (carbon/PPS) thermoforming, Struct. Control Health Monit. 18 (2011) 769–780.
[3] J. Fernández-Pérez, J.L. Cantero, J. Díaz-Álvarez, M.H. Miguélez, Influence of cutting parameters on tool wear and hole quality in composite aerospace components drilling, Compos. Struct. 178 (2017) 157–161.
[4] X. Sourd, R. Zitoune, L. Crouzeix, M. Coulaud, D. Lamouche, Influence of the damage generated by abrasive water jet texturing on the tensile static and fatigue behaviour of 3D woven composite in the context of repair, Compos. A Appl. Sci. Manuf. 149 (2021) 106567, https://doi.org/10.1016/j.compositesa:2021.106567.
[5] M. Romanowski, C. Łukianowicz, M. Sutowska, W. Zawadka, D.Y. Pimenov, K. Nadolny, Assessment of the Technological Quality of X5CRNI18-10 Steel Parts after Laser and Abrasive Water Jet Cutting Using Synthetic Index of Technological Quality, Materials 14 (2021) 4801.
[6] M. Sutowska, W. Kapłonek, D.Y. Pimenov, M.K. Gupta, M. Mia, S. Sharma, Influence of Variable Radius of Cutting Head Trajectory on Quality of Cutting Kerf in the Abrasive Water Jet Process for Soda-Lime Glass, Materials 13 (2020) 4277.
[7] G. Kim, B.R. Denos, R. Sterkenburg, Influence of different piercing methods of abrasive waterjet on delamination of fiber reinforced composite laminate, Compos. Struct. 240 (2020) 112065.
[8] H. Ho-Cheng, A failure analysis of water jet drilling in composite laminates, Int. J. Mach. Tools Manuf. 30 (1990) 423–429.
[9] D.K. Shanmugam, S.H. Masood, An investigation on kerf characteristics in abrasive waterjet cutting of layered composites, J. Mater. Process. Technol. 209 (2009) 3887–3893.
[10] I.W. Mm, A.I. Azmi, C.C. Lee, A.F. Mansor, Kerf taper and delamination damage minimization of FRP hybrid composites under abrasive water-jet machining, Int. J. Adv. Manuf. Technol. 94 (2018) 1727–1744.
[11] A. Dhanawade, S. Kumar, Experimental study of delamination and kerf geometry of carbon epoxy composite machined by abrasive water jet, J. Compos. Mater. 51 (2017) 3373–3390.
[12] M. Hashish, Machining of advanced composites with abrasive-waterjets, Mach. Compos. (1988) 1–18.
[13] K. Colligan, M. Ramulu, D. Arola, Asme, D. Materials, D. Production Engineering, Investigation of Edge Quality and Ply Delamination in Abrasive Waterjet Machining of Graphite/Epoxy, in: Winter annual meeting, Machining of advanced composites, ASME, New Orleans, LA, 1993, pp. 167–186.
[14] J. Schwartzentruber, M. Papini, J.K. Spelt, Characterizing and modelling delamination of carbon-fiber epoxy laminates during abrasive waterjet cutting, Compos. A Appl. Sci. Manuf. 112 (2018) 299–314.
[15] J. Schwartzentruber, J.K. Spelt, M. Papini, Modelling of delamination due to hydraulic shock when piercing anisotropic carbon-fiber laminates using an abrasive waterjet, Int. J. Mach. Tools Manuf 132 (2018) 81–95.
[16] M. Li, M. Huang, X. Yang, S. Li, K. Wei, Experimental study on hole quality and its impact on tensile behavior following pure and abrasive waterjet cutting of plain woven CFRP laminates, Int. J. Adv. Manuf. Technol. 99 (2018) 2481–2490.
[17] J.N. Nyaboro, M.A. Ahmed, H. El-Hofy, M. El-Hofy, Fluid-structure interaction modeling of the abrasive waterjet drilling of carbon fiber reinforced polymers, J. Manuf. Processes 58 (2020) 551–562.
[18] M. Junkar, B. Jurisevic, M. Fajdiga, M. Grah, Finite element analysis of single-particle impact in abrasive water jet machining, Int. J. Impact Eng. 32 (2006) 1095–1112.
[19] K. Dadkhahipour, T. Nguyen, J. Wang, Mechanisms of channel formation on glasses by abrasive waterjet milling, Wear 292–293 (2012) 1–10.
[20] X.u. Zhao, A. Fourie, C.-C. Qi, Mechanics and safety issues in tailing-based backfill: A review, Int. J. Miner. Metall. Mater. 27 (9) (2020) 1165–1178.
[21] D. Petković, M. Barjaktarovic, S. Milošević, N. Denić, B. Spasić, J. Stojanović, M. Milovancevic, Neuro fuzzy estimation of the most influential parameters for Kusum biodiesel performance, Energy 229 (2021) 120621.
[22] D. Petković, Ž. Ćojbašič, V. Nikolić, Adaptive neuro-fuzzy approach for wind turbine power coefficient estimation, Renew. Sustain. Energy Rev. 28 (2013) 191–195.
[23] P.R. Vundavilli, M.B. Parappagoudar, S.P. Kodali, S. Benguluri, Fuzzy logic-based expert system for prediction of depth of cut in abrasive water jet machining process, Know.-Based Syst. 27 (2012) 456–464.
[24] Z. Hashin, Failure Criteria for Unidirectional Fiber Composites, J. Appl. Mech. 47 (1980) 329–334.
[25] C.-Y. Hsu, C.-C. Liang, T.-L. Teng, A.-T. Nguyen, A numerical study on high-speed water jet impact, Ocean Eng. 72 (2013) 98–106.
[26] D. Systemes, Abaqus 6.14 Documentation. Simulia Co. Providence, RI, USA, 2014.
[27] G. Pasken, J. Ma, M. McQuilling, M.P. Jahan, Numerical Modeling of a Pure Water Jet Machining of Ti-6Al-4V and Al 6061–T6 Using ABAQUS and Smoothed Particle Hydrodynamics, ASME 2018 International Mechanical Engineering Congress and Exposition, 2018.
[28] Y. Feng, W. Jianming, L. Feihong, Numerical simulation of single particle acceleration process by SPH coupled FEM for abrasive waterjet cutting, Int. J. Adv. Manuf. Technol. 59 (2012) 193–200.
[29] M. Ali Kouka, F. Abbassi, M. Demiral, F. Ahmad, M. Soula, F. Al Housni, Al Housni, Behaviour of woven-ply PPS thermoplastic laminates with interacting circular holes under tensile loading: An experimental and numerical study, Eng. Fract. Mech. 251 (2021) 107802, https://doi.org/10.1016/j.engfracmech.2021.107802.
[30] L. Jebri, F. Abbassi, M. Demiral, M. Soula, F. Ahmad, Experimental and numerical analysis of progressive damage and failure behavior of carbon Woven-PPS, Compos. Struct. 243 (2020) 112234.
[31] D. Feng, F. Aymerich, Finite element modelling of damage induced by low-velocity impact on composite laminates, Compos. Struct. 108 (2014) 161–171.
[32] O.T. Topac, B. Gozluklu, E. Gurses, D. Coker, Experimental and computational study of the damage process in CFRP composite beams under low-velocity impact, Compos. A Appl. Sci. Manuf. 92 (2017) 167–182.
[33] M. Demiral, F. Kadioglu, V.V. Silberschmidt, Size effect in flexural behaviour of unidirectional GFRP composites, J. Mech. Sci. Technol. 34 (2020) 5053–5061.